International Journal of Refrigeration 145 (2023) 59–67

Contents lists available at ScienceDirect

International Journal of Refrigeration

journal homepage: www.elsevier.com/locate/ijrefrig

Efficient modulation of the magnetocaloric refrigerator capacity

Modulation efficace de la puissance du réfrigérateur magnétocalorique

M. Masche [a], J. Liang [a,b], K. Engelbrecht [a,*], C.R.H. Bahl [a]

[a] Department of Energy Conversion and Storage, Technical University of Denmark (DTU), Anker Engelunds Vej B301, 2800 Kgs., Lyngby, Denmark
[b] Department of Civil and Mechanical Engineering, Technical University of Denmark (DTU), Nils Koppels Allé B403, 2800 Kgs., Lyngby, Denmark

ARTICLE INFO

Keywords:
Magnetocaloric refrigeration
Partial load
Coefficient of performance
Efficiency
Experiment
Froid magnétique
capacité partielle
Coefficient de performance
Expérimenter

Mots clés:
Froid magnétocalorique
Charge partielle
Coefficient de performance
Efficacité
Expérimentation

ABSTRACT

Magnetocaloric energy conversion devices (e.g., room air conditioners and household refrigerators) have the potential to significantly reduce the emissions associated with refrigerant leakage into the atmosphere but still have lower efficiencies compared to mature vapor compression systems. The efficiency of a magnetocaloric cooling device derives not only from its design characteristics (e.g., solid refrigerant, hydraulic system, and magnet system) and its operating temperature span but also from its modulating capability. Owing to the lack of experimental data regarding this topic, the advantage of modulating the cooling capacity (i.e., the part-load performance) of an active magnetic regenerator prototype is demonstrated experimentally for the first time. The capacity modulation is carried out by means of regulating both the cycle frequency of the device and the volumetric flow rate of the heat transfer fluid. At a 14 K temperature span and a 1.4 Hz frequency, the magnetocaloric refrigerator prototype using 3.8 kg of gadolinium provided a maximum cooling capacity of 452 W with an appreciable coefficient of performance of 3.2, which corresponds to a second-law efficiency of 15.5 %. At part-load operating conditions, the device can produce a cooling capacity of 245 W with an increased second-law efficiency of 29.7 %, or a coefficient of performance of 6.2, making it more competitive with traditional vapor compression systems. In future studies, the experimental data obtained may be implemented in a dynamic building energy model to quantify the energy-saving benefits of part-load operation by estimating the overall system efficiency during a typical cooling season.

1. Introduction

The latest Intergovernmental Panel on Climate Change report on global warming and climate change underlined the urgency of accelerating the pace of cutting greenhouse gas emissions to avoid warming of 1.5°C or 2°C and mitigate environmental concerns such as ocean acidification, sea level rise, heavy rainfall, and extreme droughts (European Commission, 2021). To tackle the dire impacts of climate change, the European Commission proposed an EU-wide greenhouse gas (GHG) emission target of at least 55 % by 2030, compared to 1990 levels, and a sustainable path towards climate neutrality by 2050 (European Commission, 2020a). Moreover, the Renewable Energy Directive established new binding targets for the EU for 2030 of at least 32 % of renewable energy sources in the EU's energy mix and a reduction of energy consumption through improvements in energy efficiency by at least 32.5 % (European Commission, 2020b). In Europe, buildings are the largest energy consumers (ca. 40 % of the EU energy consumption) and account for 36 % of the GHG emissions (European Commission, 2019). Thus, the building sector is crucial to achieving the EU's climate targets.

The modernization of the building sector in light of technological improvements will help the EU boost the energy efficiency of buildings. In existing buildings, the vast majority of cooling and heating systems like refrigerators, heat pumps, and air conditioners employ the vapor compression cycle, which has caused unpredicted global environmental impacts such as ozone layer depletion and global warming due to its gaseous refrigerant being released into the atmosphere as direct emissions (Catalini et al., 2019). However, direct emissions produced over the course of the system lifetime only contribute to a small proportion of the total lifetime emissions of a vapor compression system, while indirect emissions mainly due to energy consumption can account for up to 90 % of the total lifetime emissions (Lee et al., 2016). The development of energy-conversion technologies with fewer harmful effects on the environment and improved energy efficiency will drastically affect the

* Corresponding author.
E-mail address: kuen@dtu.dk (K. Engelbrecht).

https://doi.org/10.1016/j.ijrefrig.2022.10.005
Received 4 July 2022; Received in revised form 23 September 2022; Accepted 9 October 2022
Available online 28 November 2022

Nomenclature

Acronyms

AMR	Active Magnetic Regenerator
DTU	Technical University of Denmark
MCM	Magnetocaloric Material
MCE	Magnetocaloric Effect

Roman symbols

c	Specific heat capacity [J•kg^{-1}•K^{-1}]
COP	Coefficient of Performance [-]
d	Diameter [mm]
f	Operating (motor) frequency [Hz]
F_b	Blow fraction [%]
p	Pressure [bar]
$\dot{Q}_c$	Cooling power [W]
T	Temperature [K]
T_{amb}	Ambient temperature [K]
T_{cold}	Cold reservoir temperature [K]
T_{hot}	Hot reservoir temperature [K]
U	Utilization factor [-]
$\dot{V}$	Volumetric flow rate [L/h]
$\dot{W}_{losses}$	Iron losses [W]
$\dot{W}_{mag}$	Magnetic power [W]
$\dot{W}_{shaft}$	Shaft power [W]
$\dot{W}_{pump}$	Pumping power [W]

Greek symbols

ΔT	Temperature span, T_{hot}-T_{cold} [K]
η_{II}	Second-law efficiency [%]
ρ	Density [kg•m^{-3}]
Γ	Shaft torque [Nm]

Subscripts

f	Fluid
s	Solid refrigerant

global energy demand and hence reduce the carbon footprint in the building sector. For this reason, conventional vapor compression technologies need to be retrofitted with more environmentally friendly refrigerants and energy-efficient versions in order to improve the sustainability of buildings.

One alternative is magnetocaloric energy conversion, which relies on utilizing the magnetocaloric effect (MCE) in solid-state magnetocaloric materials (MCMs) (Pecharsky and Gschneidner Jr, 1999). In an adiabatic process, the MCE is indicated by a temperature change due to a varying magnetic field. When an external magnetic field is applied adiabatically, the disorder of the magnetic spins reduces, thereby decreasing the magnetic entropy. The lowering of the magnetic entropy leads to an increase in the lattice and electronic entropy contributions to remain a constant total entropy, causing the material to heat up. After the heat is removed from the system, adiabatic demagnetization restores the magnetic entropy, thereby reducing the material temperature (Smith et al., 2012). The MCE near room temperature in most MCMs is limited to a maximum adiabatic temperature change of less than 8 K, which is too small to attain a useful temperature span in a cooling device (Lyubina, 2017). The active magnetic regenerator (AMR) concept, where the MCM acts as a refrigerant and a regenerator at the same time (Barclay, 1982), is an efficient process to achieve cooling at higher useful temperature spans (Zimm, 2016).

The development of AMR systems that employ alternative heat transfer fluids (HTF) and solid refrigerants with no ozone depletion or direct global warming potential and potentially higher efficiencies than vapor compression systems has gained large research interest in recent years (Kitanovski et al., 2015a). A comprehensive list of magnetocaloric prototypes can be found in Refs. (Greco et al., 2019; Trevizoli et al., 2016a; Zimm et al., 2018). Most AMR devices utilize spheres of gadolinium (Gd) as the MCM, which has a Curie temperature near 293 K, and Gd is often considered the benchmark refrigerant for room-temperature applications (Smith et al., 2012). Extensive research has been carried out on efficiency improvements of AMR systems by modeling and testing new MCMs (Engelbrecht et al., 2013; Jacobs et al., 2013; Lei et al., 2016; Neves Bez et al., 2016; Pecharsky et al., 2016; Richard et al., 2004; Tegus et al., 2002; Tušek et al., 2014; Vieira et al., 2021), improved geometries of the MCM (Aprea et al., 2018; Kamran et al., 2017; T. Lei et al., 2017; Li et al., 2019; Liang et al., 2021; Plait et al., 2022; Trevizoli et al., 2017; Tušek et al., 2013; Vuarnoz and Kawanami, 2012; You et al., 2018; Zhang et al., 2021), composites of Gd/first-order phase transition alloys (Chung et al., 2022; Dedruktip et al., 2022), geometries of the AMR bed (Dall'Olio et al., 2017b; Olio et al., 2015), non-water HTFs (Chiba et al., 2017; Kamran et al., 2017; Z. Lei et al., 2017; Mugica et al., 2017), different thermodynamic AMR cycles (He et al., 2013; Kitanovski et al., 2014; Plaznik et al., 2013; Romero Gómez et al., 2013), different magnetic field profiles (Bjørk and Engelbrecht, 2010) and fluid flow profiles (Fortkamp et al., 2018; Nakashima et al., 2018a, 2018b; Teyber et al., 2017), advanced permanent magnet configurations (Arnold et al., 2014; Bahl et al., 2012; Bjørk et al., 2010; Insinga et al., 2016; Lionte et al., 2021; Okamura and Hirano, 2013; Trevizoli et al., 2015; You et al., 2016a), heat transfer enhancements (Chen et al., 2014; You et al., 2017, 2016b), control strategies (Aprea et al., 2017; Huang et al., 2019; Qian et al., 2019, 2018), and improved AMR designs with reduced thermal parasitic losses (Eriksen et al., 2016; Lozano et al., 2013; Trevizoli et al., 2016b). Despite the large efforts that have been made to improve the efficiency of magnetocaloric devices, their second-law efficiencies are less than those of ultra-high efficiency vapor compression systems (up to 50 % (Steven Brown and Domanski, 2014)). In addition, AMR cooling devices need to operate at high frequencies to remain economically competitive with vapor compression systems (Egolf et al., 2004).

Generally, to make magnetocaloric cooling devices more economical, their specific cooling capacity must be increased. An efficient way to do so is to increase the operating frequency of the device (Egolf et al., 2010; Kitanovski et al., 2015b; Masche et al., 2021), but only up to the frequencies at which the required temperature span along the AMR can be established and exceeded (Kitanovski et al., 2015b). There are also several technical issues that limit the machine operation at high frequencies, such as limited HTF properties, limited stability of the MCM, and limitations given by flow channels, fluid flow switching armatures, etc. (Egolf et al., 2010). Several studies also indicate that for each frequency, there is an optimum utilization factor that ensures the optimum AMR cooling operation (Egolf et al., 2010; Kitanovski et al., 2015b). Higher operating frequencies are linked to a lower coefficient of performance (*COP*), and hence a lower device efficiency. This is mostly driven by the fact that the optimum utilization is approximately constant with respect to frequency, and as the frequency increases, the fluid flow rate must also increase to maintain the utilization, which increases the viscous dissipation due to pumping losses. Concurrently, the number of transfer units of the regenerator decreases, resulting in lower regenerator effectiveness and lower overall efficiency (Masche et al., 2021). Hence, the utilization factor and operating frequency play an important role in the cost and energy efficiency of an AMR device.

One attempt to improve the efficiency of AMR systems and compete with vapor compression systems is to consider the operation of the AMR

system at part-load conditions. Qian et al. (Qian et al., 2018) proposed a feedback control strategy to automatically tune the fluid flow rate and cycle frequency for capacity modulation under part-load operating conditions by numerical simulation. The authors reported a 500 % enhancement of the *COP* for an air-conditioning system when operated under part-load conditions, demonstrating the large energy-saving potential for part-load operation. However, experimental confirmation of the simulation results is still lacking. Here, for the first time, we present an experimental study on the effect of capacity modulation of an AMR cooling device by regulating the fluid flow rate and cycle frequency on the energy efficiency and energy-saving potential when the device operates under partial load. Hence, the study attempts to optimize the efficiency of an AMR cooling device by realizing partial load operating conditions.

2. Experimental

2.1. Apparatus for part-load testing

The performance demonstration and operation under part-load conditions were carried out in a rotary multi-bed AMR system. The main design features of the AMR system are illustrated in Fig. 1a. Table 1 also gives an overview of the main AMR design components. Each of the 13 trapezoid-shaped regenerator beds comprises 295 g of commercial-grade Gd arranged as a packed sphere bed with particles having diameters of between 0.35 and 0.71 mm. A continuously operating centrifugal pump delivers the overall flow of HTF to the AMR device and connects the AMR beds with the cold reservoir (connected to the heat source) and hot reservoir (connected to the heat sink). From a hydraulic point of view, each AMR bed is connected to a fluid-collecting manifold and a fluid-distributing manifold on the hot side and similarly on the cold side. More details about the AMR design can be found in Refs. (Dall'Olio et al., 2021, 2017a).

The fluid flow in the cold-to-hot direction (i.e., the cold blow) and hot-to-cold direction (i.e., the hot blow) through each regenerator bed can be controlled using two sets of solenoid valves installed on the regenerator hot outlet and inlet, respectively. This allows a constant circulation of the HTF. In particular, after magnetization of the AMR bed, heat is transferred from the solid refrigerant to the HTF due to the MCE. The warm HTF is then displaced towards the hot reservoir, where it rejects heat into the hot reservoir heat exchanger (or heat sink) that can keep a fixed hot reservoir temperature (T_{hot}) controlled by a commercial chiller. In the other half of the AMR cycle, after the removal of the magnetic field, the temperature of the MCM is lowered so that heat is transferred from the HTF to the MCM. The HTF is then displaced towards the cold reservoir, where heat is absorbed from an electric circulation heater (or heat source) that controls the cold reservoir temperature (T_{cold}). The fluid flow path through an AMR bed is illustrated in Fig. 1b. The temperature span (ΔT) of the AMR device can then

Table 1
AMR system specifications.

Property	Value
Magnet system	
Magnet type	Rotating
Number of poles	Two
Magnet material	NdFeB
Total magnet volume	10532 cm^3
Maximum magnetic flux density	1.44 T
Air gap	34 mm
Hydraulic system	
Flow circuit	Parallel flow
Heat transfer fluid	Deionized water mixed with 10 vol.% mono-ethylene glycol
Fluid flow control	Solenoid valves
Fluid flow transport	Centrifugal pump
Regenerator characteristics	
Bed geometry	Trapezoid
Bed volume	60.30 cm^3, 0.059 m long, 0.017 m height
Bed porosity	0.38
Number of beds	13 (fixed)
Number of layers	1
Bed type	Spheres
MCM	Gadolinium
MCM mass	295 g (3.83 kg in total)
MCM particle diameters	0.35-0.71 mm
MCM specific entropy change	3.5 J/kg/K at a peak temperature of 290.5 K at 1 T

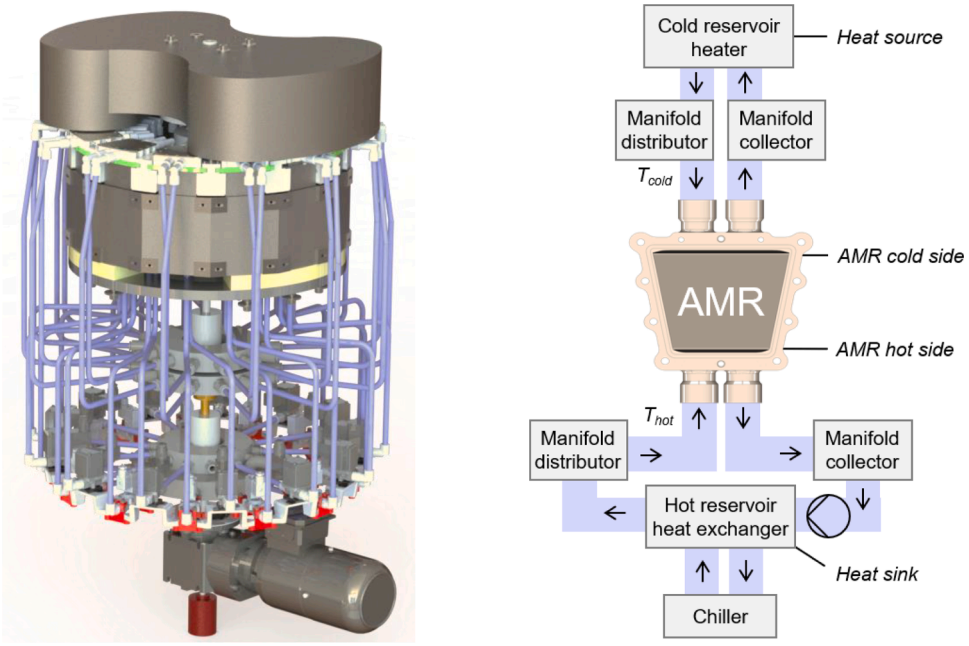

Fig. 1. (a) Photo-realistic rendering of the CAD model of the rotary AMR system developed at DTU Energy. (b) Schematic of the AMR experimental setup.

be defined as the difference between the hot and cold reservoir temperatures.

Resistance thermometers and pressure transmitters were installed inside the four manifolds to measure the temperature and pressure, respectively. The temperature of the HTF exiting the regenerator at the cold outlet was measured using thermocouples. This particular temperature can indicate how well the flow among the regenerator beds is balanced, as demonstrated previously (D. Eriksen et al., 2016; Masche et al., 2022). A torque meter was installed on the magnet shaft to measure the power needed to rotate the magnetic circuit ($\dot{W}_{shaft}$). The position of the rotating magnet was monitored by an absolute rotary encoder mounted on the shaft. The information from the encoder angle reading was used to open and close the solenoid valves at the relevant times. The fluid flow rate was measured using a low range (0.5–10 L/min) and a high range (5.7–56.8 L/min) flow meter. The accuracies of the measurement instruments are given in (M. Masche et al., 2021).

2.2. Test procedure

In a previous study, running the AMR device at a cycle frequency of 1.4 Hz appeared to be the optimum frequency in terms of achieving the maximum cooling capacity (Masche et al., 2022). Hence, it may be considered the full-load cooling capacity of the AMR device. Therefore, initially, a set of experiments was performed at 1.4 Hz and different volumetric fluid flow rates (presented as the utilization factors) to achieve steady-state full-load operation, which was selected as a reference condition for comparison with part-load operation. Steady-state operating conditions were achieved when the standard deviation of the measured reservoir temperature span was below 0.05 K for more than about 2 min. The experimental data were then averaged over a period of 10 min.

The utilization factor (U) was used to allow a performance comparison with other magnetic refrigeration systems. The cooling performance of AMR systems has been shown to be optimum at a specific value of U for a given regenerator geometry, frequency, and temperature span (Nakashima et al., 2018a, 2018b; Trevizoli et al., 2016c). Generally, higher values of U are desired when lower temperature spans are demanded for the AMR application (Velázquez et al., 2014). U is a dimensionless number and is given by:

$$U = \frac{\rho_f \, c_f \, \dot{V}}{2 f \, m_s \, c_s} \quad \text{(Eq. 1)}$$

Where c_s represents the average specific heat capacity of Gd, which is set to $c_s = 380$ J kg^{-1} K^{-1}, as per (Vieira et al., 2021). m_s is the total mass of MCM, which is 3.83 kg. c_f, ρ_f, and $\dot{V}$ are the fluid specific heat capacity, the fluid density, and the volumetric fluid flow rate, respectively.

All experiments were performed at constant reservoir temperatures. The hot reservoir temperature controlled by the chiller was kept constant at a value of approximately 301 K, whilst the cold reservoir temperature controlled by the heater was about 287 K, leading to a constant nominal temperature span of 14 K. The average fluid blow fraction (F_b), which is the ratio of a single fluid blow period to the whole AMR cycle period (Fortkamp et al., 2018), was set to 36 % in the cold-to-hot and hot-to-cold directions. In addition, the magnetic field profile is centered on the fluid flow profile, i.e., the mid-points of the periods of cold/hot fluid blow and magnetization/demagnetization are aligned. The cold and hot fluid blow periods are identical, and each of the beds has the same fluid flow profile.

Previously, we also reported variations in the fluid temperatures at the cold outlets of the 13 beds as a result of flow imbalances in the multi-bed AMR system, possibly due to different hydraulic resistances through the beds (Masche et al., 2022). As a result, the AMR cooling performance was shown to be reduced. Fluid flow imbalances between the beds could be corrected by adjusting the fluid blow fractions of individual beds, leading to lower cold outlet fluid temperature variations, which had a favorable effect on the AMR cooling performance. The experimental data presented in this work are hence based on an adjusted flow to obtain the best AMR cooling performance under different operating conditions.

The full-load operation experiments were performed to obtain a cooling performance map (*COP* vs. the cooling capacity) that was later compared with the performance maps at part-load operating conditions. Part-load operating conditions were achieved by varying the cycle (or AMR) frequency and the volumetric flow rate of the HTF, whilst keeping both the reservoir temperature span and fluid blow fractions similar to the full-load conditions. In total, three frequencies and fourteen different utilizations were tested, giving a total of 42 experiments. The operating test conditions are summarized in Table 2.

The cooling power ($\dot{Q}_c$) was calculated from the temperature difference of the fluid between the inlet and outlet of the cold reservoir heater (ΔT_{cold}) multiplied by the volumetric flow rate and properties of the HTF (see). The *COP* of the AMR device, which was determined by , takes into account the magnetic power ($\dot{W}_{mag}$) and pumping power ($\dot{W}_{pump}$) as the input power contributions, and hence the work due to the AMR internal operation. The latter power contribution is the power needed to overcome the viscous losses of the working fluid. In , p_1, p_2, p_3, and p_4 represent the fluid pressures measured inside the four manifolds. The $\dot{W}_{mag}$ term is calculated by subtracting the drivetrain power losses ($\dot{W}_{losses}$) from the $\dot{W}_{shaft}$, and it is given in . The $\dot{W}_{losses}$ is a function of the AMR frequency (f_{AMR}) and includes eddy current power losses and bearing frictional losses, as demonstrated in Refs. (M. Masche et al., 2021; Masche et al., 2022). The f_{AMR} is twice the operating frequency (f), as the rotating magnet assembly generates two high field regions. The definition of the *COP* of the ideal (Carnot) AMR device (COP_{ideal}) using leads to the determination of the second-law efficiency (η_{II}) that accounts for all external irreversibilities and quantifies the actual performance of the AMR system compared to an ideal system. The valve power consumption is external to the AMR operation and hence not included in the *COP* equation.

$$\dot{Q}_c = \dot{V} \, \rho_f \, c_f \, \Delta T_{cold} \quad \text{(Eq. 2)}$$

$$COP = \frac{\dot{Q}_c}{\dot{W}_{mag} + \dot{W}_{pump}} \quad \text{(Eq. 3)}$$

$$\dot{W}_{pump} = \dot{V}(p_1 - p_2 + p_3 - p_4) \quad \text{(Eq. 4)}$$

$$\dot{W}_{mag} = \dot{W}_{shaft} - \dot{W}_{losses} \quad \text{(Eq. 5)}$$

$$\dot{W}_{shaft} = \pi f_{AMR} \Gamma \quad \text{(Eq. 6)}$$

$$COP_{ideal} = \frac{T_{cold}}{T_{hot} - T_{cold}} \quad \text{(Eq. 7)}$$

$$\eta_{II} = \frac{COP}{COP_{ideal}} \quad \text{(Eq. 8)}$$

The relative standard uncertainties of the utilization factor, cooling capacity, pumping power, magnetic power, temperature span, *COP*, and second-law efficiency were estimated to be approximately 1 %, 10 %, 3

Table 2
Operating conditions.

Parameter	Value
AMR cycle	Reversed Brayton
Volumetric flow rate, $\dot{V}$	250–1700 L/h
Cycle (AMR) frequency, f_{AMR}	0.5 Hz; 1.1 Hz; 1.4 Hz
Average cold and hot fluid blow fractions, F_b	36 %
Average ambient temperature, T_{amb}	296 K
Average hot reservoir temperature, T_{hot}	301 K
Average cold reservoir temperature, T_{cold}	287 K

%, 2 %, 1 %, 10 %, and 10 %, respectively, as per the Taylor Series Method (Coleman and Steele, 2018). The experimental data for the *COP* of the AMR device are presented for four systems: one system where only the shaft work to rotate the regenerator and pump are included, and the component inefficiencies external to the regenerator are excluded (referred to as the idealized system) and three systems where irreversibilities due to transmission losses and pumping losses are included. In the latter ones, three classes of efficiency equipment were considered to assess the *COP* of realistic AMR systems utilizing i) low-efficiency (LE) equipment, ii) medium-efficiency (ME) equipment, and iii) high-efficiency (HE) equipment. For each efficiency class, representative efficiencies are chosen. Table 3 summarizes the different efficiency classes and their design irreversibilities.

3. Results and discussion

The effect of cooling capacity modulation for the AMR system operating at steady-state conditions is presented in Fig. 2. At a cycle frequency of 1.4 Hz and a fixed temperature span of 14 K, the system achieved a peak cooling capacity of around 452 W at a utilization factor of about 0.33, which appears to be the optimum at the given frequency after adjusting only the volumetric flow rate. In addition to adjusting only the volumetric flow rate (and hence the utilization factor), the cycle frequency can also be controlled to modulate the cooling capacity of the system. It can be seen that the optimum utilization to reach the maximum cooling capacity changes with both the utilization and frequency, keeping both the temperature span and average blow fractions constant. It should be noted that the valve adjustments made to keep the outlet temperatures from each regenerator more uniform can change the utilization where the maximum cooling power occurs at each frequency. The plot also demonstrates the strong dependency of the cooling power on the utilization factor, which was also reported by Trevizoli et al. (2016b) and Lozano et al. (2016). Hence, the amount of heat transfer fluid and cycle frequency must be explored thoroughly to obtain maximum cooling capacities.

Fig. 3a shows that the magnetocaloric device at full-load and at $U = 0.33$, where it produced the highest cooling power, was not operating most energy efficiently, indicated by a *COP* lower than the maximum value. In other words, the maximum cooling *COP* of the system occurred at lower utilization than the maximum cooling capacity, and this trend was similar for the different load conditions. This was also the case regardless of whether the AMR system was considered an idealized or realistic system with three different efficiency classes. For instance, for the system with HE equipment, the maximum cooling capacity was achieved with a *COP* of 2.5 ($U = 0.33$), which was below the maximum *COP* of 3.2 ($U = 0.14$). The reason why the AMR operates more efficiency at lower utilization is due to both the reduced magnetic and pumping power input as a result of a lower pressure drop across the system (Masche et al., 2022), and a more efficient heat transfer. It is interesting to note that the peak of the *COP* for the ideal system was 4.6 at $U = 0.14$ at 1.4 Hz and 5.3 at $U = 0.12$ at 1.1 Hz (Fig. 3b), respectively, slightly shifted towards larger utilization when a system with realistic efficiency equipment was considered. This utilization shift was not observed for a system running at a cycle frequency of 0.5 Hz (Fig. 3b). Additionally, there are only small differences between the three equipment cases with respect to the system efficiency, while the assumption of an ideal system can largely overestimate the cooling efficiency of the device. As expected, the system with LE components produced cooling with the lowest efficiency. Fig. 3d also plots the cooling performance for all three cycle frequencies for an ideal AMR system, indicating that the system COP will decrease gradually with increasing the cycle frequency.

Table 3
Overview of the four efficiency classes.

System irreversibilities	Ideal system	LE system	ME system	HE system
Electric motor efficiency, η_M [%]	100	78	85	92
Motor drive efficiency, η_D [%]	100	95	95	95
Pump efficiency, η_P [%]	100	75	80	85

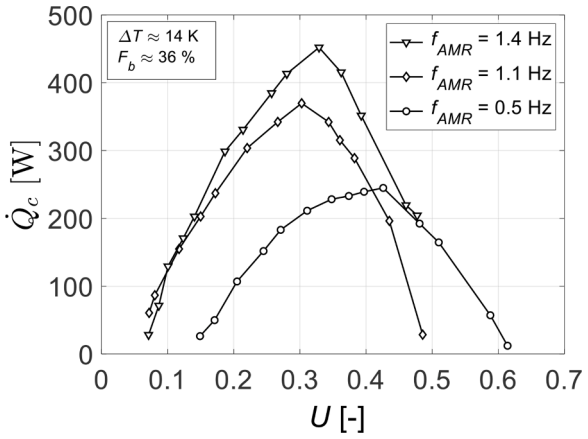

Fig. 2. Cooling capacity of the AMR device at steady-state full-load and part-load operating conditions.

Fig. 4a-b illustrate how the AMR cooling efficiency is affected by varying the electric motor efficiency or pumping efficiency whilst keeping the efficiency of the pump or motor constant at low or high levels. The operating conditions in all four cases were the same with a cycle frequency of 0.5 Hz, a constant temperature span of 14 K, and average blow fractions in the cold and hot blow directions of 36 %. The general trend was that the electric motor efficiency appeared to be the dominating component in the AMR system, as changing from HE motor efficiency ($\eta_{M,HE}$) to LE motor efficiency ($\eta_{M,LE}$) resulted in a greater reduction of the AMR cooling efficiency than changing from HE pumping efficiency ($\eta_{P,HE}$) to LE pumping efficiency ($\eta_{P,LE}$). Interestingly, the effect of varying the pumping efficiency on the cooling *COP is* nearly negligible. Previous studies that have shown that the magnetic power (Masche et al., 2022) or shaft power (Fortkamp et al., 2018) are the dominating power input of an AMR system, indicating that inefficiency variations in the motor drive system can have a greater impact on the AMR cooling efficiency than inefficiency variations in the pump.

The cooling performance maps (cooling *COP* vs. cooling capacity) for the AMR system at full-load and part-load operating conditions are shown in Fig. 5a-d. It is clear that cooling performance maps were very sensitive to the efficiency class equipment that was used in the AMR system. The cooling *COP* substantially decreased, as the efficiencies of both the electric motor and pump were reduced, while providing the same cooling load as for the idealized system. This can be identified as a flattening of the performance maps in the plots. Finally, the plots stress that for each of the four studied systems, the combined adjustment of the cycle frequency and volumetric fluid flow rate (or utilization factor) are crucial modulation strategies to realize part-load operation of an AMR system with enhanced energy-saving potential.

4. Conclusion

The cooling performance of a rotary multi-bed active magnetic regenerator device was investigated from an in-depth experimental analysis at full and part-load operating conditions. The cooling power and efficiency of the device at full-load operating conditions were compared to those at part-load conditions at a constant temperature span of 14 K and constant fluid blow fractions. The part-load conditions were achieved by tuning both the cycle frequency and the flow rate of the heat transfer fluid. The study stresses the importance of cooling

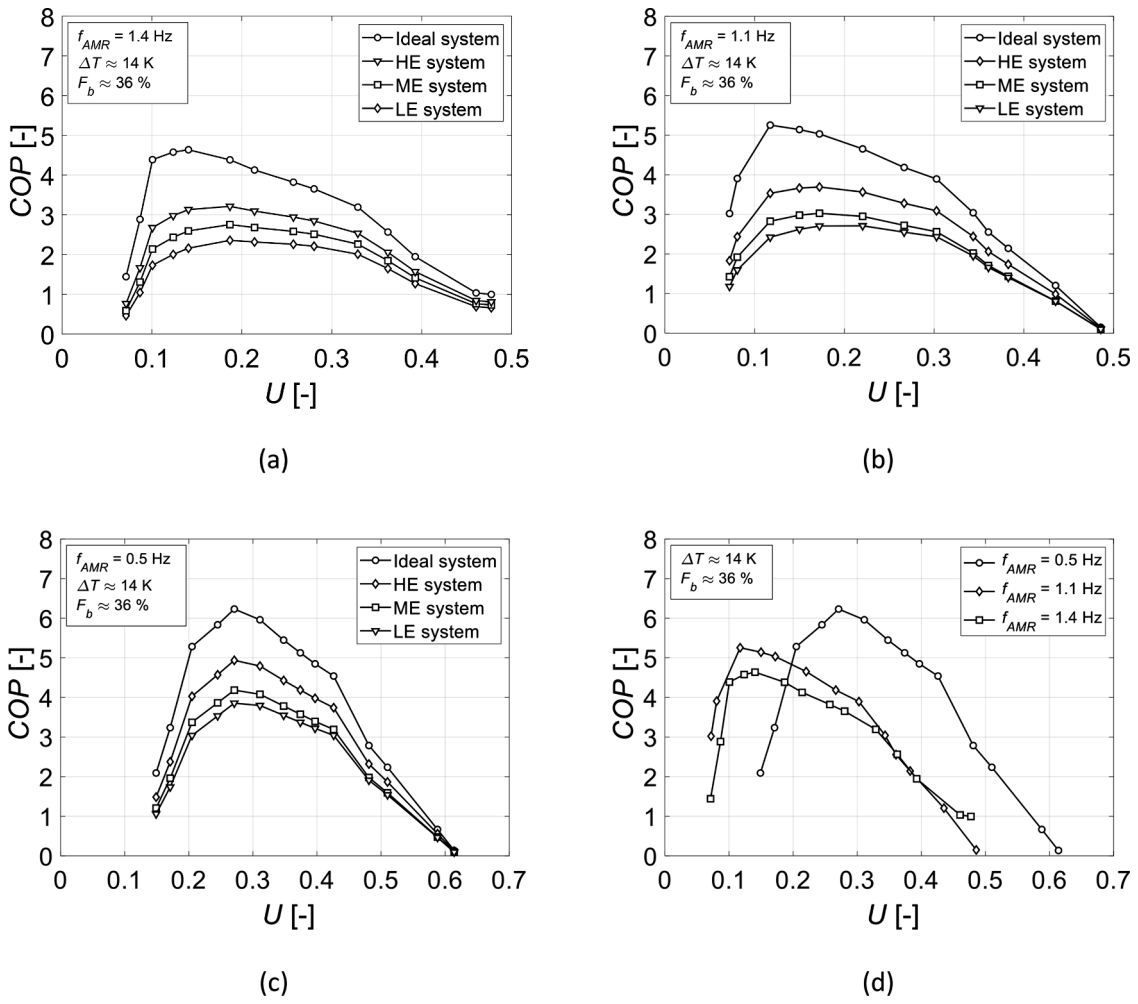

Fig. 3. Cooling performance of the AMR system for different efficiency classes at (a) 1.4 Hz, (b) 1.1 Hz, (c) 0.5 Hz, and (d) Cooling performance for all three frequencies for the ideal AMR system.

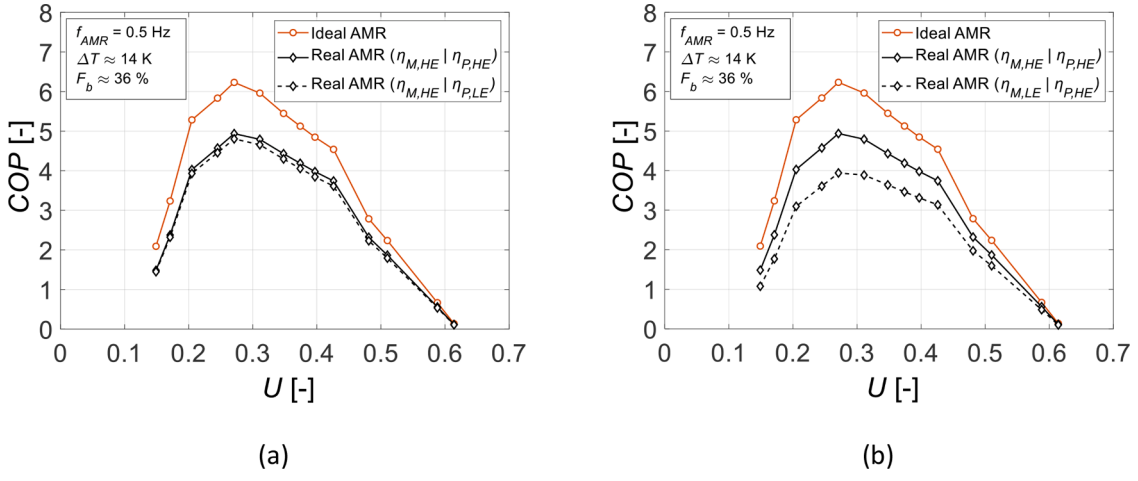

Fig. 4. (a) Effect of varying the pump efficiency on the AMR cooling performance, whilst keeping a high motor efficiency ($\eta_{M,HE}$) or low motor efficiency ($\eta_{M,LE}$). (b) Effect of varying the motor efficiency on the AMR cooling performance, whilst keeping a high pump efficiency ($\eta_{P,HE}$) or low pump efficiency ($\eta_{P,LE}$).

capacity modulation for enhancing the device efficiency at part load, hence providing a large energy-saving potential. A reduction of the cooling capacity to 54 % of the maximum load almost doubles the cooling efficiency. In addition, to obtain a designed cooling capacity of around 200 W, the efficiency of the device can be largely improved when switching from full load to part load operating conditions. Further research may be conducted to investigate the on-off cycling behavior of the active magnetic regenerator device that could account for performance degradation from start-up losses.

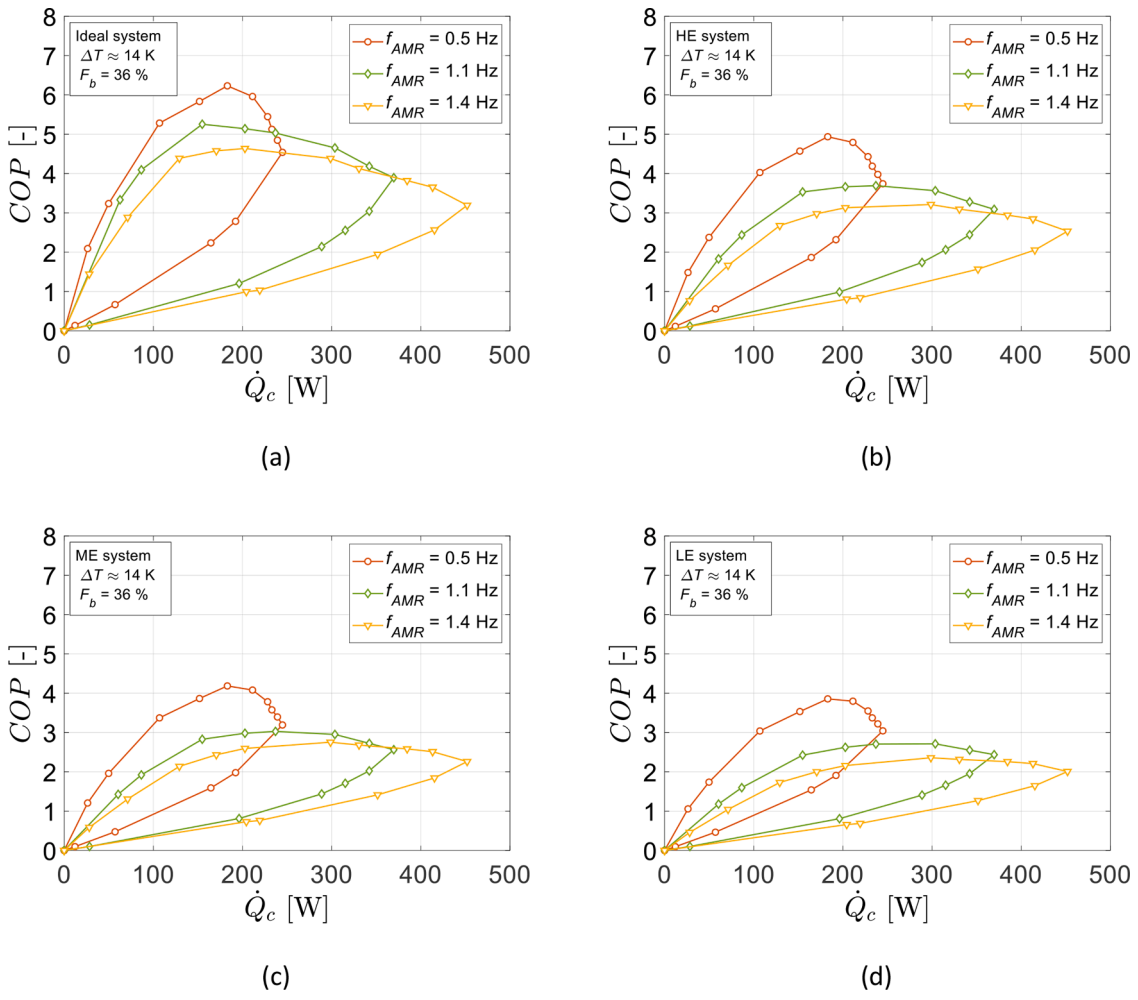

Fig. 5. Cooling performance maps of the AMR device at full and part-load operation for (a) an ideal system, (b) HE system, (c) ME system, (d) and LE system.

Declaration of Competing Interest

The authors declare that they have no known competing financial interests or personal relationships that could have appeared to influence the work reported in this paper.

Acknowledgements

This work was in part financed by the RES4Build project, which received funding from the European Union's Horizon 2020 research and innovation program under grant agreement No. 814865.

References

Aprea, C., Greco, A., Maiorino, A., 2017. An application of the artificial neural network to optimise the energy performances of a magnetic refrigerator. Int. J. Refrig. 82, 238–251. https://doi.org/10.1016/j.ijrefrig.2017.06.015.

Aprea, C., Greco, A., Maiorino, A., Masselli, C., 2018. Energy performances and numerical investigation of solid-state magnetocaloric materials used as refrigerant in an active magnetic regenerator. Therm. Sci. Eng. Prog. 6, 370–379. https://doi.org/10.1016/j.tsep.2018.01.006.

Arnold, D.S., Tura, A., Ruebsaat-Trott, A., Rowe, A., 2014. Design improvements of a permanent magnet active magnetic refrigerator. Int. J. Refrig. 37, 99–105. https://doi.org/10.1016/j.ijrefrig.2013.09.024.

Bahl, C.R.H., Velázquez, D., Nielsen, K.K., Engelbrecht, K., Andersen, K.B., 2012. High performance magnetocaloric perovskites for magnetic refrigeration. Appl. Phys. Lett. 121905. https://doi.org/10.1063/1.3695338.

Barclay, J.A., 1982. Use of a ferrofluid as the heat-exchange fluid in a magnetic refrigerator. J. Appl. Phys. 53, 2887–2894. https://doi.org/10.1063/1.331069.

Bjørk, R., Bahl, C.R.H., Smith, A., Pryds, N., 2010. Review and comparison of magnet designs for magnetic refrigeration. Int. J. Refrig. 33, 437–448. https://doi.org/10.1016/j.ijrefrig.2009.12.012.

Bjørk, R., Engelbrecht, K., 2010. The influence of the magnetic field on the performance of an active magnetic regenerator (AMR). Int. J. Refrig. 34, 192–203. https://doi.org/10.1016/j.ijrefrig.2010.07.004.

Catalini, D., Emaikwu, N., Hwang, Y., Radermacher, R., Takeuchi, I., 2019. Elastocaloric cooling 37, 29–32.

Chen, Z., Utaka, Y., Tasaki, Y., 2014. Measurement and numerical simulation on the heat transfer characteristics of reciprocating flow in microchannels for the application in magnetic refrigeration. Appl. Therm. Eng. 65, 150–157. https://doi.org/10.1016/j.applthermaleng.2014.01.007.

Chiba, Y., Smaili, A., Sari, O., 2017. Enhancements of thermal performances of an active magnetic refrigeration device based on nanofluids. Mechanics 23, 31–38. https://doi.org/10.5755/j01.mech.23.1.13452.

Chung, K., Shinde, K.P., Kang, K.H., Lee, A.Y., Park, J., Kim, J.-W., 2022. Magnetocaloric Properties of a Wire Composite of La(Fe,Mn,Si)13-H Alloy Powders in a Gd Cylindrical Tube. Available SSRN 4148263.

Coleman, H.W., Steele, W.G., 2018. Experimentation, Validation, and Uncertainty Analysis for Engineers. John Wiley & Sons.

Dall'Olio, S., Eriksen, D., Engelbrecht, K., Insinga, A.R., Bahl, C.R.H., 2017a. Design, enhanced thermal and flow efficiency of a 2 kW active magnetic regenerator. In: 9th World Conference on Experimental Heat Transfer, Fluid Mechanics and Thermodynamics, pp. 1–10.

Dall'Olio, S., Lei, T., Engelbrecht, K., Bahl, C.R.H., 2017b. The effect of tapering on a magnetocaloric regenerator bed. Int. J. Refrig. 84, 300–308. https://doi.org/10.1016/j.ijrefrig.2017.08.012.

Dall'Olio, S., Masche, M., Liang, J., Insinga, A.R., Eriksen, D., Bjørk, R., Nielsen, K.K., Barcza, A., Vieyra, H.A., Beek, N.v., Bez, H.N., Engelbrecht, K., Bahl, C.R.H., 2021. Novel design of a high efficiency multi-bed active magnetic regenerator heat pump. Int. J. Refrig. 132, 243–254. https://doi.org/10.1016/j.ijrefrig.2021.09.007.

Dedruktip, N., Panjatewakub, P., Lupponglung, V., Na Wichean, T., Matan, K., Techapiesancharoenkij, R., 2022. Performance comparison of Ga and Ga/La alloy layered active magnetic regeneration beds in a rotary magnetic refrigeration prototype. Mater. Today Proc. 65, 2340–2346. https://doi.org/10.1016/j.matpr.2022.05.230.

Egolf, P.W., Gonin, C., Kitanovski, A., 2010. Central Magnetic Cooling and Refrigeration Machines (Chiller) and their Assessment.

Egolf, P.W.P., Gendre, F., Kitanovski, A., Sari, O., 2004. Machbarkeitsstudie für magnetische Wärmepumpen: Anwendungen in der Schweiz. Umgebungswärme, Wärme-Kraft.
Engelbrecht, K., Nielsen, K.K., Bahl, C.R.H., Carroll, C.P., Van Asten, D., 2013. Material properties and modeling characteristics for MnFeP 1 - X As x materials for application in magnetic refrigeration. J. Appl. Phys. 113, 173510 https://doi.org/10.1063/1.4803495.
Eriksen, Dan, Engelbrecht, K., Bahl, C.R.H., Bjørk, R., 2016. Exploring the efficiency potential for an active magnetic regenerator. Sci. Technol. Built Environ. 22, 527–533. https://doi.org/10.1080/23744731.2016.1173495.
Eriksen, D., Engelbrecht, K., Bahl, C.R.H., Bjørk, R., Nielsen, K.K., 2016. Effects of flow balancing on active magnetic regenerator performance. Appl. Therm. Eng. 103, 1–8. https://doi.org/10.1016/j.applthermaleng.2016.03.001.
European Commission, 2021. No Title [WWW Document]. URL. https://www.ipcc.ch/2021/08/09/ar6-wg1-20210809-pr/.
European Commission, 2020a. Eu [WWW Document]. URL. https://eur-lex.europa.eu/legal-content/EN/TXT/?uri=CELEX:52020DC0562.
European Commission, 2020b. No Title [WWW Document]. URL. https://ec.europa.eu/clima/eu-action/climate-strategies-targets/2030-climate-energy-framework_en.
European Commission, 2019. No Title [WWW Document]. URL. https://ec.europa.eu/energy/topics/energy-efficiency/energy-efficient-buildings/energy-performance-buildings-directive_en.
Fortkamp, F.P., Eriksen, D., Engelbrecht, K., Bahl, C.R.H., Lozano, J.A., Barbosa Jr, J.R., 2018. Experimental investigation of different fluid flow profiles in a rotary multi-bed active magnetic regenerator device. Int. J. Refrig. 91, 46–54. https://doi.org/10.1016/j.ijrefrig.2018.04.019.
Greco, A., Aprea, C., Maiorino, A., Masselli, C., 2019. A review of the state of the art of solid-state caloric cooling processes at room-temperature before 2019. Int. J. Refrig. 106, 66–88. https://doi.org/10.1016/j.ijrefrig.2019.06.034.
He, X.N., Gong, M.Q., Zhang, H., Dai, W., Shen, J., Wu, J.F., 2013. Design and performance of a room-temperature hybrid magnetic refrigerator combined with Stirling gas refrigeration effect. Int. J. Refrig. 6, 2–8. https://doi.org/10.1016/j.ijrefrig.2013.03.014.
Huang, B., Lai, J.W., Zeng, D.C., Zheng, Z.G., Harrison, B., Oort, A., van Dijk, N.H., Brück, E., 2019. Development of an experimental rotary magnetic refrigerator prototype. Int. J. Refrig. 104, 42–50. https://doi.org/10.1016/j.ijrefrig.2019.04.029.
Insinga, A.R., Bjork, R., Smith, A., Bahl, C.R.H., 2016. Optimally segmented permanent magnet structures. IEEE Trans. Magn. 52, 1–6. https://doi.org/10.1109/TMAG.2016.2593685.
Jacobs, S., Auringer, J., Boeder, A., Chell, J., Komorowski, L., Leonard, J., Russek, S., Zimm, C., 2013. The performance of a large-scale rotary magnetic refrigerator. Int. J. Refrig. 37, 84–91. https://doi.org/10.1016/j.ijrefrig.2013.09.025.
Kamran, M.S., Ahmad, H.O., Asim, M., Hayat, N., 2017. Performance analysis of amicrochannel amr magnetic refrigerator using different heat transfer fluids. World Appl. Sci. J. 35, 1658–1665. https://doi.org/10.5829/idosi.wasj.2017.1658.1665.
Kitanovski, A., Plaznik, U., Tomc, U., Poredoš, A., 2015a. Present and future caloric refrigeration and heat-pump technologies. Int. J. Refrig. 57, 288–298. https://doi.org/10.1016/J.IJREFRIG.2015.06.008.
Kitanovski, A., Plaznik, U., Tušek, J., Poredoš, A., 2014. New thermodynamic cycles for magnetic refrigeration. Int. J. Refrig. 37, 28–35. https://doi.org/10.1016/j.ijrefrig.2013.05.014.
Kitanovski, A., Tušek, J., Tomc, U., Plaznik, U., Ožbolt, M., Poredoš, A., 2015b. Magnetocaloric Energy Conversion: From Theory to Applications. Springer.
Lee, H., Troch, S., Hwang, Y., Radermacher, R., 2016. LCCP evaluation on various vapor compression cycle options and low GWP refrigerants. Int. J. Refrig. 70, 128–137. https://doi.org/10.1016/j.ijrefrig.2016.07.003.
Lei, T., Engelbrecht, K., Nielsen, K.K., Neves Bez, H., Bahl, C.R.H., 2016. Study of multi-layer active magnetic regenerators using magnetocaloric materials with first and second order phase transition. J. Phys. D. Appl. Phys. 49 https://doi.org/10.1088/0022-3727/49/34/345001.
Lei, T., Engelbrecht, K., Nielsen, K.K., Veje, C.T., 2017. Study of geometries of active magnetic regenerators for room temperature magnetocaloric refrigeration. Appl. Therm. Eng. 111, 1232–1243. https://doi.org/10.1016/j.applthermaleng.2015.11.113.
Lei, Z., Raebiger, D., Eckert, S., Eckert, K., 2017. Liquid metal based magnetic cooling: velocity measurements. Magnetohydrodynamics 53, 403–410.
Li, Z., Shen, J., Li, K., Gao, X., Guo, X., Dai, W., 2019. Assessment of three different gadolinium-based regenerators in a rotary-type magnetic refrigerator. Appl. Therm. Eng. 153, 159–167. https://doi.org/10.1016/j.applthermaleng.2019.02.100.
Liang, J., Engelbrecht, K., Nielsen, K.K., Loewe, K., Vieyra, H., Barcza, A., Bahl, C.R.H., 2021. Performance assessment of a triangular microchannel active magnetic regenerator. Appl. Therm. Eng. 186, 116519 https://doi.org/10.1016/j.applthermaleng.2020.116519.
Lionte, S., Risser, M., Muller, C., 2021. A 15kW magnetocaloric proof-of-concept unit: Initial development and first experimental results. Int. J. Refrig. 122, 256–265. https://doi.org/10.1016/j.ijrefrig.2020.09.019.
Lozano, J.A., Capovilla, M.S., Trevizoli, P.V., Engelbrecht, K., Bahl, C.R.H., Barbosa Jr, J. R., 2016. Development of a novel rotary magnetic refrigerator. Int. J. Refrig. 68, 187–197. https://doi.org/10.1016/j.ijrefrig.2016.04.005.
Lozano, J.A., Engelbrecht, K., Bahl, C.R.H., Nielsen, K.K., Eriksen, D., Olsen, U.L., Barbosa Jr, J.R., Smith, A., Prata, A.T., Pryds, N., 2013. Performance analysis of a rotary active magnetic refrigerator. Appl. Energy 111, 669–680. https://doi.org/10.1016/j.apenergy.2013.05.039.
Lyubina, J., 2017. Magnetocaloric materials for energy efficient cooling. J. Phys. D. Appl. Phys. 50, 053002 https://doi.org/10.1088/1361-6463/50/5/053002.
Masche, M, Ianniciello, L., Tušek, J., Engelbrecht, K., 2021. Impact of hysteresis on caloric cooling performance. Int. J. Refrig. 121, 302–312. https://doi.org/10.1016/j.ijrefrig.2020.10.012.
Masche, M., Liang, J., Dall'Olio, S., Engelbrecht, K., Bahl, C.R.H., 2021. Performance analysis of a high-efficiency multi-bed active magnetic regenerator device. Appl. Therm. Eng. 199, 117569 https://doi.org/10.1016/j.applthermaleng.2021.117569.
Masche, M., Liang, J., Engelbrecht, K., Bahl, C.R.H., 2022. Performance assessment of a rotary active magnetic regenerator prototype using gadolinium. Appl. Therm. Eng. 204, 117947 https://doi.org/10.1016/j.applthermaleng.2021.117947.
Mugica, I., Roy, S., Poncet, S., Bouchard, J., Nesreddine, H., 2017. Exergy Analysis of a Parallel-Plate Active Magnetic Regenerator with Nanofluids. Entropy 19, 464. https://doi.org/10.3390/e19090464.
Nakashima, A.T.D., Dutra, S.L., Trevizoli, P.V., Barbosa Jr, J.R., 2018a. Influence of the flow rate waveform and mass imbalance on the performance of active magnetic regenerators. Part II: Numerical simulation. Int. J. Refrig. 93, 159–168. https://doi.org/10.1016/j.ijrefrig.2018.07.005.
Nakashima, A.T.D., Dutra, S.L., Trevizoli, P.V., Barbosa Jr, J.R., 2018b. Influence of the flow rate waveform and mass imbalance on the performance of active magnetic regenerators. Part I: Experimental analysis. Int. J. Refrig. 93, 236–248. https://doi.org/10.1016/j.ijrefrig.2018.07.004.
Neves Bez, H., Navickaitė, K., Lei, T., Engelbrecht, K., Barcza, A., Bahl, C.R.H., 2016. Epoxy-bonded La(Fe,Mn,Si)13Hz as a multi layered active magnetic regenerator. In: 7th International Conference on Caloric Cooling. Torino, Italy. https://doi.org/10.18462/iir.thermag.2016.0147.
Okamura, T., Hirano, N., 2013. Improvement of the Performance of Room Temperature Magnetic Refrigerator using Gd-alloy. J. Japan Soc. Appl. Electromagn. Mech. 21, 10–14. https://doi.org/10.14243/jsaem.21.10.
Olio, S.D., Lei, T., Engelbrecht, K., Bahl, C.R.H., 2015. Numerical Simulation of an Tapered Bed AMR.
Pecharsky, V.K., Cui, J., Johnson, D.D., 2016. (Magneto)caloric refrigeration: is there light at the end of the tunnel? Philos. Trans. R. Soc. A Math. Phys. Eng. Sci. 374, 20150305 https://doi.org/10.1098/rsta.2015.0305.
Pecharsky, V.K., Gschneidner Jr, K.A., 1999. Magnetocaloric effect and magnetic refrigeration. J. Magn. Magn. Mater. 200, 44–56. https://doi.org/10.1016/S0304-8853(99)00397-2.
Plait, A., de Larochelambert, T., Giurgea, S., Espanet, C., 2022. Experimental validation of a multiphysics modeling for a magnetocaloric bench. Appl. Therm. Eng. 211, 118415 https://doi.org/10.1016/j.applthermaleng.2022.118415.
Plaznik, U., Tušek, J., Kitanovski, A., Poredoš, A., 2013. Numerical and experimental analyses of different magnetic thermodynamic cycles with an active magnetic regenerator. Appl. Therm. Eng. 59, 52–59. https://doi.org/10.1016/j.applthermaleng.2013.05.019.
Qian, S., Yuan, L., Yu, J., 2019. An online optimum control method for magnetic cooling systems under variable load operation. Int. J. Refrig. 97, 97–107. https://doi.org/10.1016/j.ijrefrig.2018.09.033.
Qian, S., Yuan, L., Yu, J., Yan, G., 2018. Variable load control strategy for room-temperature magnetocaloric cooling applications. Energy 153, 763–775. https://doi.org/10.1016/j.energy.2018.04.104.
Richard, M.A., Rowe, A.M., Chahine, R., 2004. Magnetic refrigeration: single and multimaterial active magnetic regenerator experiments. J. Appl. Phys. 95, 2146–2150. https://doi.org/10.1063/1.1643200.
Romero Gómez, J., Ferreiro Garcia, R., De Miguel Catoira, A., Romero Gómez, M., 2013. Magnetocaloric effect: a review of the thermodynamic cycles in magnetic refrigeration. Renew. Sustain. Energy Rev. 17, 74–82. https://doi.org/10.1016/j.rser.2012.09.027.
Smith, A., Bahl, C.R.H., Bjørk, R., Engelbrecht, K., Nielsen, K.K., Pryds, N., 2012. Materials challenges for high performance magnetocaloric refrigeration devices. Adv. Energy Mater. 2, 1288–1318. https://doi.org/10.1002/aenm.201200167.
Steven Brown, J., Domanski, P.A., 2014. Review of alternative cooling technologies. Appl. Therm. Eng. 64, 252–262. https://doi.org/10.1016/j.applthermaleng.2013.12.014.
Tegus, O., Brück, E., Buschow, K.H.J., de Boer, F.R., 2002. Transition-metal-based magnetic refrigerants for room-temperature applications. Nature 415, 150–152. https://doi.org/10.1038/415150a.
Teyber, R., Trevizoli, P.V., Niknia, I., Christiaanse, T.V., Govindappa, P., Rowe, A., 2017. Experimental performance investigation of an active magnetic regenerator subject to different fluid flow waveforms. Int. J. Refrig. 74, 38–46. https://doi.org/10.1016/j.ijrefrig.2016.10.001.
Trevizoli, P.V., Christiaanse, T.V., Govindappa, P., Niknia, I., Teyber, R., Barbosa Jr, J.R., Rowe, A., 2016a. Magnetic heat pumps: An overview of design principles and challenges. Sci. Technol. Built Environ. 22, 507–519. https://doi.org/10.1080/23744731.2016.1171632.
Trevizoli, P.V., Lozano, J.A., Peixer, G.F., Barbosa Jr, J.R., 2015. Design of nested Halbach cylinder arrays for magnetic refrigeration applications. J. Magn. Magn. Mater. 395, 109–122. https://doi.org/10.1016/j.jmmm.2015.07.023.
Trevizoli, P.V., Nakashima, A.T., Barbosa Jr, J.R., 2016b. Performance evaluation of an active magnetic regenerator for cooling applications – part II: Mathematical modeling and thermal losses. Int. J. Refrig. 72, 206–217. https://doi.org/10.1016/j.ijrefrig.2016.07.010.
Trevizoli, P.V., Nakashima, A.T., Peixer, G.F., Barbosa, J.R., 2017. Performance assessment of different porous matrix geometries for active magnetic regenerators. Appl. Energy 187, 847–861. https://doi.org/10.1016/j.apenergy.2016.11.031.
Trevizoli, P.V., Nakashima, A.T., Peixer, G.F., Barbosa Jr, J.R., 2016c. Performance evaluation of an active magnetic regenerator for cooling applications – part I : Experimental analysis and thermodynamic performance. Int. J. Refrig. 72, 192–205. https://doi.org/10.1016/j.ijrefrig.2016.07.009.

Tušek, J., Kitanovski, A., Tomc, U., Favero, C., Poredoš, A., 2014. Experimental comparison of multi-layered La-Fe-Co-Si and single-layered Gd active magnetic regenerators for use in a room-temperature magnetic refrigerator. Int. J. Refrig. 37, 117–126. https://doi.org/10.1016/j.ijrefrig.2013.09.003.

Tušek, J., Kitanovski, A., Zupan, S., Prebil, I., Poredoš, A., 2013. A comprehensive experimental analysis of gadolinium active magnetic regenerators. Appl. Therm. Eng. 53, 57–66. https://doi.org/10.1016/j.applthermaleng.2013.01.015.

Velázquez, D., Palacios, E., Estepa, L., Burriel, R., 2014. A versatile magnetic refrigeration demonstrator. In: 6th IIF-IIR International Conference on Magnetic Refrigeration, p. 2.

Vieira, B.P., Bez, H.N., Kuepferling, M., Rosa, M.A., Schafer, D., Plá Cid, C.C., Vieyra, H. A., Basso, V., Lozano, J.A., Barbosa Jr, J.R., 2021. Magnetocaloric properties of spheroidal La(Fe,Mn,Si)13Hy granules and their performance in epoxy-bonded active magnetic regenerators. Appl. Therm. Eng. 183, 116185 https://doi.org/10.1016/j.applthermaleng.2020.116185.

Vuarnoz, D., Kawanami, T., 2012. Numerical analysis of a reciprocating active magnetic regenerator made of gadolinium wires. Appl. Therm. Eng. 37, 388–395. https://doi.org/10.1016/j.applthermaleng.2011.11.053.

You, Y., Guo, Y., Xiao, S., Yu, S., Ji, H., Luo, X., 2016a. Numerical simulation and performance improvement of a multi-polar concentric Halbach cylindrical magnet for magnetic refrigeration. J. Magn. Magn. Mater. 405, 231–237. https://doi.org/10.1016/j.jmmm.2015.12.077.

You, Y., Wu, Z., Chen, P., Ji, H., Zeng, X., Xu, X., Dai, F., 2018. Improving magnetic refrigerator performances by enhancing convection heat transfer with staggered twin-wedged elements. Appl. Therm. Eng. 132, 423–431. https://doi.org/10.1016/j.applthermaleng.2017.12.127.

You, Y., Wu, Z., Xiao, S., Li, H., Xu, X., 2017. A comprehensive two-dimensional numerical study on unsteady conjugate heat transfer in magnetic refrigerator with Gd plates. Int. J. Refrig. 79, 217–225. https://doi.org/10.1016/j.ijrefrig.2017.04.014.

You, Y., Yu, S., Tian, Y., Luo, X., Huang, S., 2016b. A numerical study on the unsteady heat transfer in active regenerator with multi-layer refrigerants of rotary magnetic refrigerator near room temperature. Int. J. Refrig. 65, 238–249. https://doi.org/10.1016/j.ijrefrig.2016.02.002.

Zhang, R., Zhang, X., Qian, M., Bahl, C.R.H., 2021. Numerical analysis of an active magnetic regenerator with parallel wire geometry based on a 1D AMR model. Int. J. Refrig. 129, 250–258. https://doi.org/10.1016/j.ijrefrig.2021.04.024.

Zimm, C., Boeder, A., Mueller, B., Rule, K., Russek, S.L., 2018. The evolution of magnetocaloric heat-pump devices. MRS Bull 43, 274–279. https://doi.org/10.1557/mrs.2018.71.

Zimm, C.B., 2016. Magnetic refrigerator design and performance. Reference Module in Materials Science and Materials Engineering. Elsevier. https://doi.org/10.1016/B978-0-12-803581-8.01709-4.